https://chemistry-europe.onlinelibrary.wiley.com/doi/full/10.1002/cssc.202001719
https://doi.org/10.1002/cssc.202001719

WILEY-VCH

SUPPLEMENTARY INFO

Enhanced N_2 fixation activity by converting Ti_3C_2 MXenes nanosheets to nanoribbons

Hua Wei [a, c], #, Qian Jiang [b], #, Claudio Ampelli [a], Shiming Chen [b], Siglinda Perathoner [a], Yuefeng Liu [b],* and Gabriele Centi [a],*

[a] Dr. H. Wei, prof. C. Ampelli, prof. S. Perathoner, prof. G. Centi
Dept.s ChimBioFarAm and MIFT,
V.le F. Stagno D'Alcontres 31,
98166 Messina, Italy.
E-mail: centi@unime.it
[b] Dr. Q. Jiang, Dr. S. Chen, prof. Y. Liu
Dalian National Laboratory for Clean Energy, Dalian Institute of Chemical Physics, Chinese Academy of Sciences,
457 Zhongshan Road, Dalian 116023, China.
E-mail: yuefeng.liu@dicp.ac.cn
[c] Dr. H. Wei
University of Lyon, Institut de Chimie de Lyon, UMR 5265 – CNRS – Université Lyon 1,
ESCPE Lyon, Laboratoire de Chimie, Catalyse, Polymères et Procédés (C2P2),
Equipe Chimie Organométallique de Surface, Villeurbanne, France
[#] These authors contributed equally to this work.

Supplementary Experimental Section

Electrocatalytic reactor

The electrocatalytic cell for the direct NH_3 synthesis from N_2 and H_2O operates at ambient temperature/ pressure.[1-3] A solid membrane-electrode assembly separates the gas and liquid hemicells, where the reduction of N_2 to ammonia (cathodic part) and the water oxidation (anodic part) reactions occur, respectively.

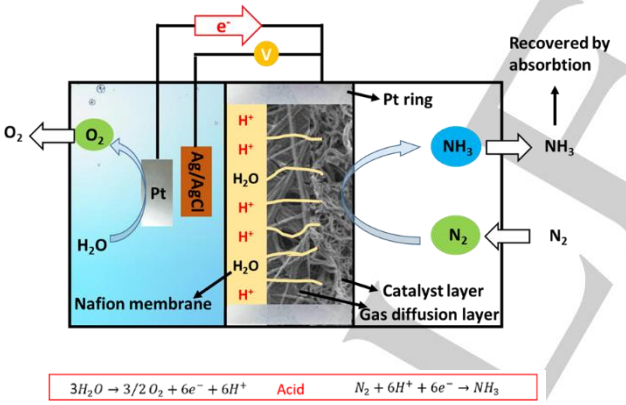

Figure S1 Schematic view of the improved design in the three-phase reactor for electrochemical ammonia synthesis. Gas chamber: cathode; working electrode is fully contact with N_2; N_2 reduced to ammonia. Electrode size about 2 cm^2. Liquid chamber: Anode; Pt as counter electrode; Water decomposition reaction. The reactant N_2 was continuously fed (20 mL min^{-1}) and the flow coming out from the electrocatalytic reactor outlet was sent to a liquid absorber containing a 0.001 M H_2SO_4 solution. Electrolyte: 0.25 M Li_2SO_4 0.5M H_2SO_4.

The anodic section contains a liquid electrolyte (0.5 M KOH) for water electrolysis to generate the protons and electrons. The protons and electrons were used in the cathodic zone for the electrocatalytic conversion of N_2 to NH_3.

This electrocatalytic reactor has a compact-design[4,5] and operates without the presence of a liquid electrolyte in the ammonia synthesis hemicell, differently from most of the other literature results. Due to its configuration, allowing continuous operations with a not energy-intensive continuous recovery of the ammonia formed, this type of reactor is indicated as gas-phase (or electrolyteless) electrocatalytic flow reactor. A main difference with respect to conventional electrochemical reactors, where the electrode is in direct contact with a liquid electrolyte, is that the gas reactant (N_2) could have a higher coverage on the electrocatalytic nanoparticles, being not limited from solubility in the electrolyte and double-charge diffusion limitations. For the case of CO_2, we demonstrated that this is an important aspect.[6]

Calculations

Ammonia formation rates were calculated using the following equation:

$$r_{NH_3}(\mu g \cdot mg_{eCAT}^{-1} \cdot h^{-1}) = \frac{x(ppm) \cdot V(l)}{M_{CAT}\ (mg) \cdot t(h)}$$

Where:
- r_{NH_3}: ammonia formation rate in $\mu g \cdot mg_{CAT}^{-1} \cdot h^{-1}$.
- x (ppm): ammonia concentration in the detection solution in ppm (mg/L)
- V (l): is volume of solution in liter.
- M_{eCAT}(mg): the amount of the electrocatalyst (mg) in the electrode
- t (h): the reaction time in hours.

Faraday efficiency of ammonia was determined using the following equations

$$FE_{NH_3}(\%) = \frac{3 \times r_{NH3}^{*}\ (mol \cdot cm^{-2} \cdot s^{-1}) \times t(s) \times S(cm^{-2}) \times F}{I(A) \times t(s)} \times 100\%$$

Where:
- F: Faraday constant,
- I(A): the average of current during the reaction,
- $P_{H_2}(\%)$: is the percentage of H_2 in the total gas flow.
- $F_{N_2}(mL/min)$: the flow of N_2, $F_{N_2}(mL/min)$=10 mL/min in the study.
- V_m: the molar volume in the standard condition (V_m = 22.4 L/mol).

Ammonia detection

The amount of ammonia formed is monitored by a highly-sensitive spectrophotometry method, which resulted preferable with respect to the alternative tested methods of ammonia detection, such as by using ammonium ion selective electrodes or using NMR.[7-9] In control experiments, we have compared the results obtained by the spectrophotometric method described below and those with NMR. Due to a discontinuous access to NMR equipment, differently from the spectrophotometric method which allow immediate analysis during the experiments, we found less reliable the NMR method, although widely used by other authors.[7-9] On the other hand, the spectrophotometric method is the established method to analyze ammonium ions in environmental analysis methods.

The method used for low ammonia concentration detection was adapted from the standard methods for analyzing ammonia in wastewater. Ammonia concentration was detected by spectrophotometry with salicylic acid, which gives better sensibility and reproducibility with respect to the alternative tested methods, such as ion selective electrode analysis (Orion™ High-Performance Ammonia Electrode 9512HPBNWP) or ammonia detection by NRM. Reproducibility tests indicate an average error of less than ±5% in the estimation of the ammonia formation rate.

Details of the spectrophotometry measurement with salicylic acid are given below. The method shows analogies with that used by Guo et al.[10] Reproducibility tests indicate an average error of less than ±5% in the estimation of the ammonia formation rate.

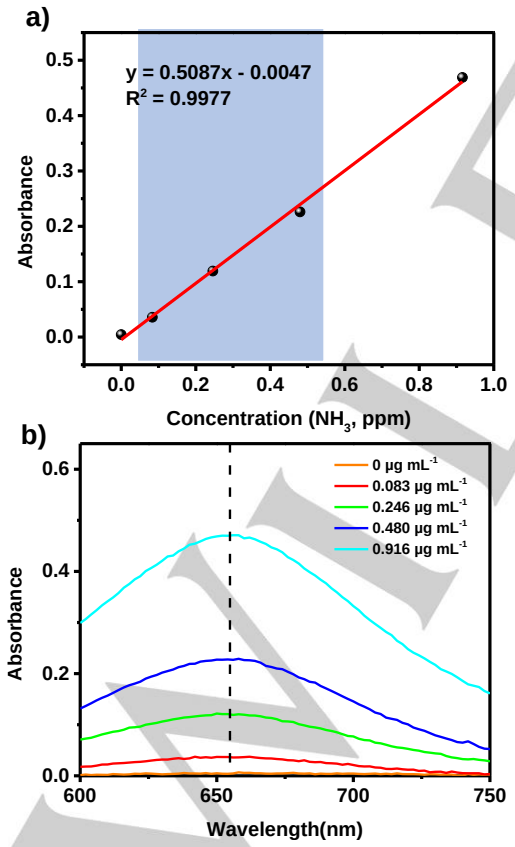

Figure S2 (a) Calibration curve used for estimation of NH_3 (b) UV-Vis absorption spectra of indophenol assays with NH_3 after incubated for 1 h at room temperature.

Regents used:

1. Coloring solution: sodium salicylate (0.4 M) and sodium hydroxide (0.32 M);
2. Oxidation solution: sodium hypochlorite (ρCl=4~4.9) and sodium hydroxide (0.75M);
3. Catalyst solution: 0.1g $Na_2[Fe(CN)_5NO]•2H_2O$ diluted to 10ml with deionized water.
4. Standard ammonium solution.

Procedure:

4 mL of sample was taken. Then 50 μL of oxidizing solution, 500 μL of coloring solution and 50 μL of catalyst solution were added respectively to the sample solution. Absorbance measurements were performed after 1 hr at λ=690 nm. The calibration curve used for estimation of NH_3 and the UV-Vis absorption spectra of indophenol assays with NH_3 after incubated for 1 h at room temperature are reported in Figures S2a and S2b, respectively.

Procedure to analyze eventual formation of hydrazine

A check for the possibility to form hydrazine (NH_2NH_2) was made using the procedure indicated by Qin et al.[11] 2 g of p-dimethylaminobenzaldehyde and 10 mL of hydrochloric acid (37%) in 100 mL of anhydrous ethanol solution are used to prepare the color reagent, 3 mL of which are with 3 mL of the liquid in the cold trap used to collect ammonia from the gas stream outlet of the gas-phase electrocatalytic reactor. After 10 min, the absorbance of 465 nm was analysed to determine whether N_2H_4 was produced. No indication of the formation of hydrazine was obtained under our experimental conditions.

Electrocatalytic tests

The electrocatalysts (about 0.2 mg/cm^2) is dispersed in ethanol containing a 10% Nafion solution (ultrasonic mixing for 90 min), up to obtain an homogenous mixture which is deposited by spray drying onto a gas-diffusion layer (GDL) which is then hot pressed to a Nafion membrane. The Nafion membrane was purified before the use. Size of the electrodes was 2 cm^2.

The electrocatalyst is located between two GDLs, one of which in contact with flowing N_2, and the other joint with the Nafion membrane. The intermediate GDL between the electrocatalyst and the Nafion is used to limit ammonia cross-over.[2] Before the tests, electrochemical CV cycles were used to reach the steady state of the electrode.

Ultrapure N_2 gas (99.9999% purity, 20 mL/min) was used in the tests, with further purification steps by passage through alkaline and acidic trap to remove possible sources of N contaminations.[12] The purification level and the absence of contaminants such as NOx was monitored by mass quadrupole and gas chromatography.

Ammonia formation and the eventual formation of hydrazine were determined as described above. H_2 formation was monitored by gas-chromatography.

Control experiments

A series of control tests were made to assure that ammonia form from N_2 feed rather than from other N sources and to verify that ammonia derives from an electrocatalytic process.

A verification was made that NOx was not present in the N_2 pure feed used in the present tests, and that contaminations by NH_3 were also not present in the feed section of the

electrocatalytic apparatus. These control experiments were further supported by switching tests with Ar feed.

In these switching-feed tests, the procedure for the electrocatalytic tests is made as described before, but only Ar is feed rather than N_2. In these conditions, no ammonia was detected. After 2h, the feed is switched to N_2 and the catalytic behavior monitored with time on stream. The results are reported in Figure S3. It is shown clearly that i) ammonia forms only when gaseous N_2 is feed and thus ammonia do not derive from contaminations by other N-compounds present in the reactor or its components, and ii) after switching to N_2 there is a stable ammonia formation for at least 2h on tests.

Control tests with labelled $^{15}N_2$ were also made to verify formation of ammonia from gas N_2,[13,14] monitoring $^{15}NH_3$ by NMR, but these tests do not provided different results. We consider preferable the procedure indicated in Figure S3, because allow a procedure protocol which can be applied to all tests.

Further control experiments regarded tests feeding N_2 and H_2, but without application of a potential to the electrocatalyst, to confirm that i) ammonia do not derive from the catalytic reduction of contaminant N-species and ii) the behaviour observed derives from the electrocatalytic reduction rather than from the catalytic reduction in presence of in-situ generated H_2.

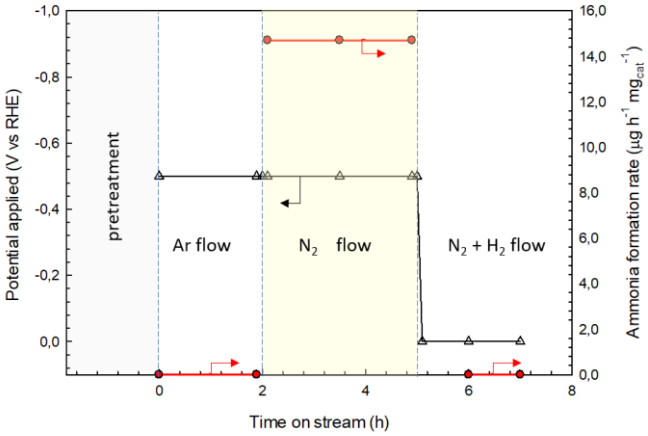

Figure S3 Experimental protocol for NRR tests: after the initial phase of pre-treatment to stabilize the electrode, the first two hours of electrocatalytic tests are made by applying the chosen potential (-0.5 V vs RHE), but feeding Ar; then , the feed is switched to N_2, maintaining constant the applied potential and ammonia formation is monitored for at least 3h; after these tests, the potential is decreased to zero, and a feed of N_2 + 5% H_2 is feed to verify the catalytic (rather than electrocatalytic) activity in ammonia formation.

Supplementary Characterization Data

The full XPS spectrum with corresponding elemental content analysis confirms the existence of C, K, O and F in Ti_3C_2 MNRs (Figure S4).

After the treatment by KOH, the intensity of the XPS Ti-F peaks decreased markedly (Figure S4), while the contents of -OH on the surface increases significantly, indicating that a large amount of -F terminal groups were replaced by hydroxyl groups and consequently the formation of O-terminated Ti_3C_2 MNRs. EDX analysis in SEM characterization of the Ti_3C_2 MNSs and Ti_3C_2 MNR samples confirm this indication (Figure S5). The comparison of the elemental composition by XPS and EDX (SEM) show that after the treatment by KOH, the Ti/C ratio increases owing to the carbon corrosion by KOH. The comparison of Ti/C ratio measured by XPS and SEM indicates a preferential surface carbon removal by the KOH treatment. The EDX comparison of MAX phase (Ti_3AlC_2) and Ti_3C_2 MNSs (Table S1) indicates also that the oxygen content is similar in these two samples.

a

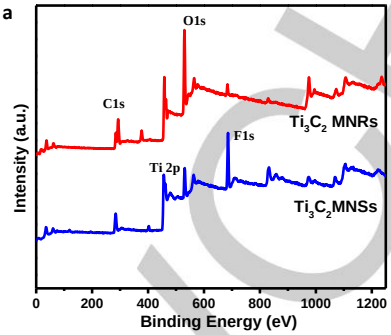

b

Element	XPS (Atomic%) Ti_3C_2 MNSs	XPS (Atomic%) Ti_3C_2 MNRs
C	38.66	17.76
O	18.68	51.38
F	21.67	3.71
Al	5.56	0
K	0	11.93
Ti	15.43	15.56

Figure S4 (a) Full XPS and (b) elemental content analysis of Ti_3C_2 MNSs and (b) Ti_3C_2 MNR.

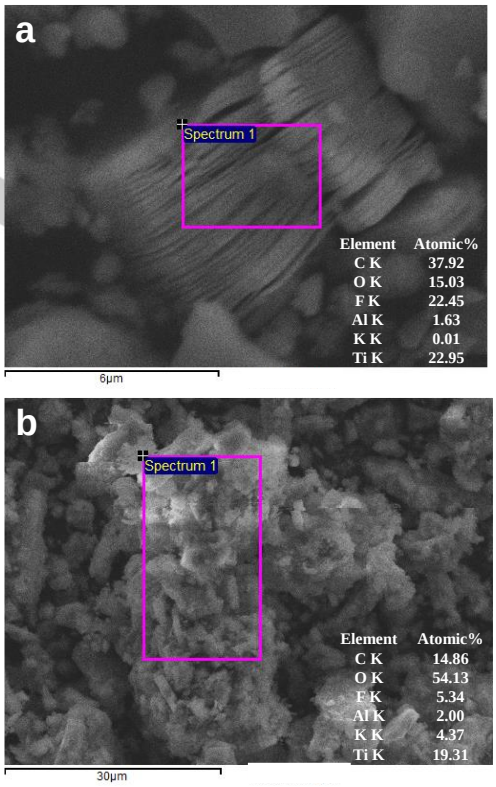

Figure S5 SEM image and EDX analysis of the marked zone in (a) Ti_3C_2 MNSs and (b) Ti_3C_2 MNR.

Table S1 Comparison of the EDX elemental composition (atomic % content) of Ti_3AlC_2 (MAX phase) and Ti_3C_2 MNS.

Element (K line)	Ti_3AlC_2 (MAX)	Ti_3C_2 MNS.
C	42.15	37.92
O	16.88	15.03
F	0.64	22.45
Al	10.02	1.63
K	0.00	0.01
Ti	30.32	22.95

Cyclic Voltammetry (CV) tests

CV tests were initially made with the MXene nano ribbon cathode to analyze the range to explore for the electrocatalytic tests. Figure S6a reports the CV curves obtained in the full range (from -1V to +1 V vs. RHE, with Figure S6b reporting an expansion in the 1V to +0.2 V vs. RHE.

Apart from a slight change in the first cycle, the CV curves are very well coincident, indicating the stability of performances during consecutive cycles.

Based on these tests, three values of potential to apply for the electrocatalytic tests could be identified: -0.2V, which corresponds to the value close to onset potential, -0.5 V corresponding to the maximum of current of the first reduction peaks, and -0.8V corresponding to the onset of a new reduction.

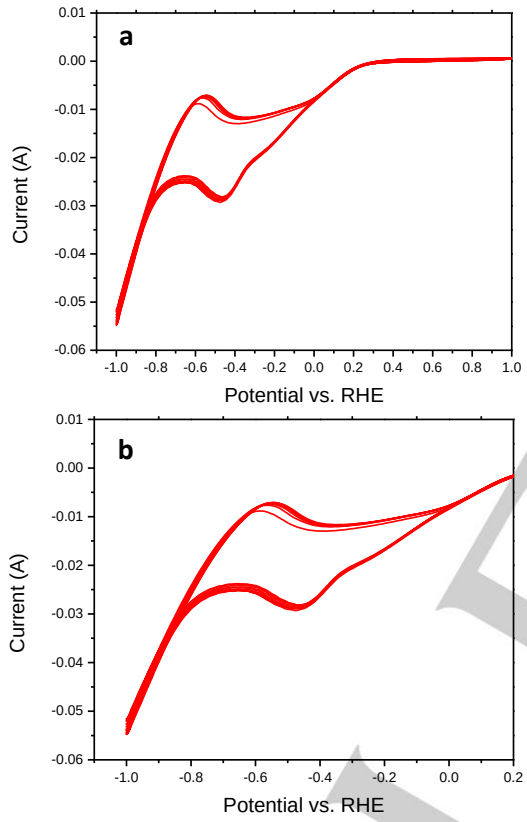

Figure S6 Cyclic voltammetry (CV) tests on Ti_3C_2 MNR. (a) full range from -1V to +1 V vs. RHE. (b) expansion in the 1V to +0.2 V vs. RHE.

Initial Tests and Stability

Based on CV results (Figure S6), initial electrocatalytic tests were made to evaluate the effect of the applied potential versus Ag AgCl in the range from -0.2V to -0.8V vs. RHE. These initial tests were performed on Ti_3C_2 MNRs. Results at intermediate voltages between those tested to not add relevant additional information. Note, in fact, that the scope of this work is not to obtain the maximum possible performances, but to understand better the effect of changing from 2D to 3D like nanostructure.

The highest NH_3 yield was obtained at −0.5 V vs RHE (Figure S7). Current density at this voltage is about -1.5 μA and remain stable for at least 3h of continuous tests (Figure S8). At more negative voltage (-0.8 V), the current density instead decreases from the initial -3.5 μA value to about -4.5 μA (after 2h), indicating thus an in-situ transformation during the electrocatalytic tests. At a voltage of -0.2 V, the current density (about -0.5 μA) is instead low, indicating low catalytic activity. Further tests were thus made at -0.5 V vs RHE. Data reported refer to the behavior determined after 3h of continuous tests.

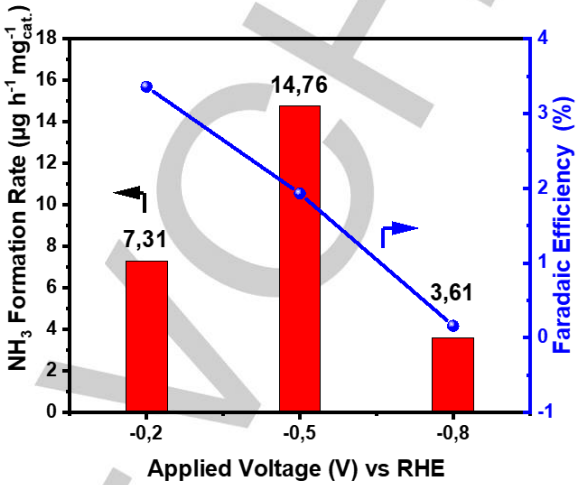

Figure S7 NH_3 formation rate and Faradaic efficiency of Ti_3C_2 MNRs at different potentials vs. Ag/AgCl.

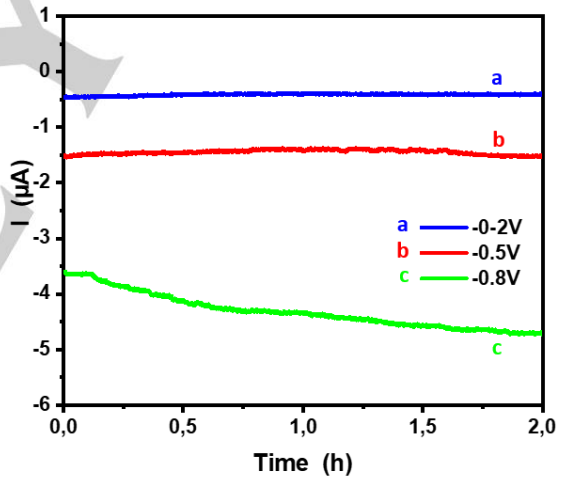

Figure S8 Time-dependent current density curves for Ti_3C_2 MNRs at different potentials vs. Ag/AgCl.

Characterization before and after the NRR catalytic tests

SEM characterization of the most active Ti_3C_2 MNRs sample, fresh and after 2h and 10h of catalytic tests are reported in Figures S9a, S9b and S9c respectively. There is no evidence of morphological changes with the time on stream of the nanoribbons, with respect to the fresh sample. These data are in well agreement with also CV experiments during extended cycling tests.

XPS Ti_{2p} spectra of fresh and used Ti_3C_2 MNRs (Figure S10) also do not evidence changes in the surface characteristics of this electrocatalyst before and after the catalytic tests, confirming the stability during NRR electrocatalytic tests.

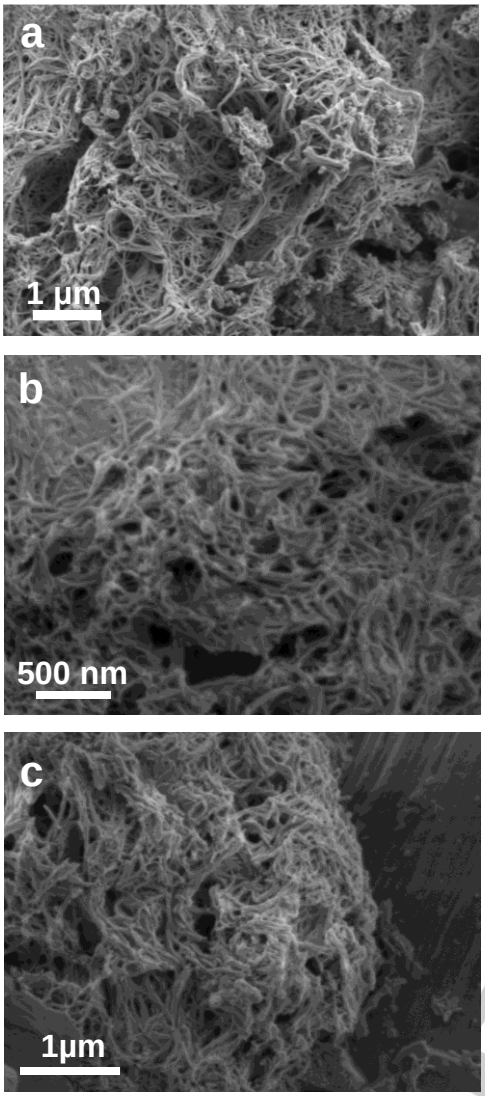

Figure S9 SEM images of Ti_3C_2 MNRs fresh (a) and after 2h (b) and 10h (c) of catalytic tests at a potential of -0.5 V vs. RHE.

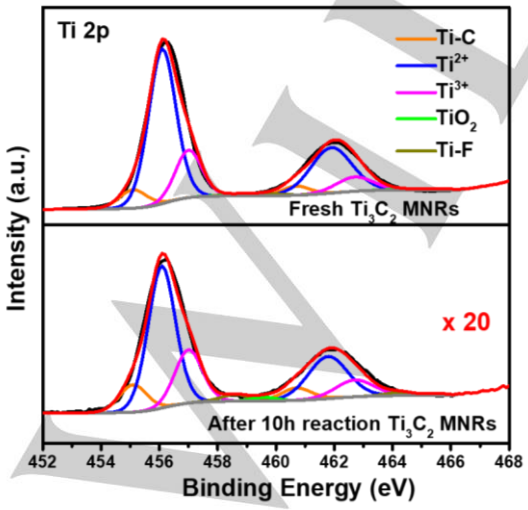

Figure S10 XPS spectra (Ti_{2p} region) of Ti_3C_2 MNRs after extended catalytic tests (10h) at a potential of -0.5 V vs. RHE.

XRD results also confirm that no structural change occur during the catalytic tests.

Comparison with state-of-the-art literature results

A comparison with state-of-the-art literature data on NRR by using as electrocatalysts (a) MXenes, (b) composite electrocatalysts based on MXenes, and selected electrocatalysts based on (c) noble metals or (d) transition metal oxides is reported in Table S2.

Table S2 Comparison with state-of-the-art representative electrocatalysts in NRR. Type of electrocatalysts: (a) MXenes, (b) modified and composite electrocatalysts based on MXenes, selected electrocatalysts based on (c) noble metals or (d) transition metal oxides.

Composition (*)	FE (%)	NH_3 Formation rate ($\mu g \cdot h^{-1} \cdot mg_{cat}^{-1}$)	Potential applied (V) and electrolyte	Ref.
(a) Pure MXenes				
Ti_3C_2 MNRs	2.0	14.8	-0.5 vs RHE 0.5 M KOH	This work
Ti_3C_2 MNSs	0.7	2.4		
$Ti_3C_2T_x$ nanosheets	2.0	6.5	-0.2 vs RHE 0.05 M H_2SO_4	15
Ti_3C_2 nanosheets	1.0	30.3	-0.3 vs RHE 0.1 M HCl	16
OH-rich $Ti_3C_2T_x$ QDs	13.3	62.9	-0.5 vs RHE 0.1 M HCl	17
OH-surface rich Ti_3C_2	7.0	1.71	-0.2 vs RHE 0.1 M KOH	18
$Ti_3C_2T_x$	1.5	22.4	-0.6 vs RHE 0.1 M HCl	19
$Ti_3C_2T_x$ nanosheet/CP	9.3	20.4	-0.4 vs RHE 0.1 M HCl	20
HF-$Ti_3C_2T_x$ nanosheets/CC	6.0	15.0	-0.3 vs RHE 0.1 M HCl	21
F-free $Ti_3C_2T_x$ nanosheets/CC	9.1	36.9		
$Ti_3C_2T_x$/CP	3.0	10.2	-0.6 vs RHE 0.1 M HCl	22
$Ti_3C_2T_x$ MXene / SSM	4.6	2.7	-0.1 vs RHE 0.5 M Li_2SO_4	23
Mo_2CT_X MXene	7.0	10.0	-0.3 vs RHE 0.5 M K_2SO_4	24
(b) Modified and composite MXenes				
MXene/ TiFeOx-700	24.4	21.9	-0.2 vs RHE 0.05 M H_2SO_4	15
1T-MoS_2/ Ti_3C_2 MXene	10.9	39.3	-0.3 vs RHE 0.1 M HCl	16
$Ti_3C_2T_x$/ TiO_2 (vacancy rich)	3.0	32.0	-0.6 vs RHE 0.1 M HCl	19
TiO_2/$Ti_3C_2T_x$ /CP	8.4	26.3	-0.6 vs RHE 0.1 M HCl	22
$Ti_3C_2T_x$ MXene / FeOOH	5.8	0.2	-0.1 vs RHE 0.5 M Li_2SO_4	23
MnO_2–$Ti_3C_2T_x$	11.9	34.1	-0.5 vs RHE 0.1 M HCl	25
Mn_3O_4/ MXene nanosheets	5.5	25.9	-0.5 vs RHE 0.1 M Na_2SO_4	26
(c) Noble-metal based electrocatalysts				
Ru-single atom Mo_2CT_X MXene	25.8	40.6	-0.3 vs RHE 0.5 M K_2SO_4	24
Ru/C	12.5	20.0		
Au nanoroads	4.0	1.6	-0.2 vs RHE 0.1 M KOH	27
Pd/C	8.2	4.5	-0.1 vs RHE 0.1M PBS	28
Rh nanosheets	0.3	23.9	-0.2 vs RHE 0.1 M KOH	29
α-Au/CeOx-RGO	10.1	8.3	-0.2 vs RHE 0.1 M HCl	30

(d) Transition metal oxide/sulphide based electrocatalysts				
Fe_2O_3/CNT 3h activated in situ	17.0	41.6	-0.5 vs RHE 0.5 M KOH	3
TiO_2/rGO	3.3	15.1	-0.9 vs RHE 0.1 M Na_2SO_4	31
amorphous $Bi_4V_2O_{11}/CeO_2$	10.1	23.2	-0.2 vs RHE 0.1 M HCl	32
Nb_2O_5 nanofibers	9.3	43.6	-0.6 vs RHE 0.1 M HCl	33
MoO_3 nanosheets	0.8	29.4	-0.5 vs RHE 0.1 M HCl	34
MnO_x nanowire	11.4	1.5	-0.5 vs RHE 0.1 M Na_2SO_4	35
Mn_3O_4 nanocube	3.0	11.6	-0.5 vs RHE 0.1 M Na_2SO_4	36
N-doped C/ Fe_3C	2.7	15.8	-0.4 vs RHE 0.01 M KOH	37
Mo- MnO_2 nanoflowers	7.7	36.6	-0.5 vs RHE 0.1 M Na_2SO_4	38
MoS_2/C_3N_4	17.8	18.5	-0.3 vs RHE -	39
Mo-SnS_2 nanosheets (&)	20.8 (-0.4V)	41.3	-0.5 vs RHE 0.5M $LiClO_4$	40
$FeMoO_4$ Nanorods	7.5	45.8	-0.5 vs RHE 0.5 M LiClO4	41

(*) T = F, OH; QDs: Quantum Dots; CP: carbon paper; CC carbon cloth; SSM: stainless steel mesh; PBS: phosphate buffer sulution. (&) with enriched S-vacancies

References

[1] S. Chen, S. Perathoner, C. Ampelli, C. Mebrahtu, D. Su, G. Centi, *Angew. Chemie Int. Ed.* **2017**, *56*, 2699.

[2] S. Chen, S. Perathoner, C. Ampelli, C. Mebrahtu, D. Su, G. Centi, *ACS Sustainable Chem. & Eng*. **2017**, 5, 7393.

[3] S. Chen, S. Perathoner, C. Ampelli, H. Wei, S. Abate, B. Zhang, G. Centi, *J. Energy Chem*., **2020**, *49*, 22.

[4] S. Perathoner, G. Centi, D. S. Su, *ChemSusChem* **2016**, 9, 345.

[5] C. Ampelli, G. Centi, R. Passalacqua, S. Perathoner, *Catal. Today* **2016**, *259*, 246

[6] B. C. Marepally, C. Ampelli, C. Genovese, T. Saboo, S. Perathoner, F. M. Wisser, L. Veyre, J. Canivet, E. A. Quadrelli, G. Centi, *ChemSusChem* **2017**, *10*, 4442-4446.

[7] R. Y. Hodgetts, A. S. Kiryutin, P. Nichols, H.-L. Du, J. M. Bakker, D. R. Macfarlane, A. N. Simonov, *ACS Energy Lett.* **2020**, *5*, 736-741.

[8] A. C. Nielander, J. M. McEnaney, J. A. Schwalbe, J. G. Baker, S. J. Blair, L. Wang, J. G. Pelton, S. Z. Andersen, K. Enemark-Rasmussen, V. Colic, et al. *ACS Catal.* **2019**, *9*, 5797-5802.

[9] G. Y. Duan, Y. Ren, Y. Tang, Y, Z, Sun, Y. M. Chen, P. Y. Wan, X. J. Yang, *ChemSusCjhem* **2020**, *13*, 88-96

[10] Y. Guo, T. Wang, Q. Yang, X. Li, H. Li, Y. Wang, T. Jiao, Z. Huang, B. Dong, W. Zhang, J. Fan, C. Zhi, *ACS Nano* **2020**, DOI: 10.1021/acsnano.0c04284

[11] B. Qin, Y. Li, Q. Zhang, G. Yang, H. Liang, F. Peng, *Nano Energy* **2020**, *68*, 104374

[12] R. Dabundo, M. F. Lehmann, L. Treibergs, C. R. Tobias, M. A. Altabet, P. H. Moisander, J. Granger, *PLOS One* **2014**, *9*, e110335.

[13] (a) S.Z., Andersen, V., Čolić, S. Yang, et al. *Nature* **2019**, *570*, 504–508. (b) L. F. Greenlee, J. N. Renner, S. L. Foster, *ACS Catal*. **2018**, *8*, 7820–7827.

[14] J. Kibsgaard, J. K. Nørskov, I. Chorkendorff, *ACS Energy Lett*. **2019**, *4*, 2986-2988

[15] Y. Guo, T.Wang, Q. Yang, X. Li, H. Li, Y. Wang, T. Jiao, Z. Huang, B. Dong, W. Zhang, Wenjun; J. Fan, C. Zhi, *ACS Nano* **2020**, Ahead of Print. DOI: 10.1021/acsnano.0c04284

[16] X. Xu, B. Sun, Z. Liang, H. Cui, J. Tian, ACS *Applied Materials & Interfaces* **2020**, *12*, 26060.

[17] Z. Jin, C. Liu, Z. Liu, J. Han, Y. Fang, Y. Han, Y. Niu, Y. Wu, C. Sun, Y. Xu, *Adv. Energy Mater*. **2020**, 10, 2000797.

[18] J. Xia, S.-Z. Yang, B. Wang, P. Wu, I. Popovs, H. Li, S. Irle, S. Dai, H. Zhu, *Nano Energy* **2020**, *72*, 104681.

[19] Y. Fang, Z, Liu, J. Han, Z. Jin, Y. Han, F. Wang, Y. Niu, Y. Wu, Y. Xu, *Adv. Energy Mater*. **2019**, *9*, 1803406.

[20] J. Zhao, L. Zhang, X. Xie, X. Li, Y. Yong, Q. Liu, W. Fang, X. Shi, G. Cui, X. Sun, *J. Mater. Chem. A* **2018**, *6*, 24031.

[21] T. Li, X. Yan, L. Huang, J. Li, L. Yao, Q. Zhu, W. Wang, W. Abbas, R. Naz, J. Gu, Q. Liu, W. Zhang, D. Zhang, *J. Chem. A: Materials for Energy and Sustainability* **2019**, *7*, 14462.

[22] J. Zhang, L. Yang, H. Wang, Z. Zhu, H. Wen, H. Feng, X. Sun, X. Guan, J. Wen, Y. Yao, *Inorg. Chem*. **2019**, *58*, 5414.

[23] Y. R. Luo, G. F. Chen, L. Ding, X. Z. Chen, L. X. Ding, H. H. Wang, *Joule* **2019**, *3*, 279.

[24] W. Peng, L. Luo, X. Xu, K. Jiang, M. Peng, D. Chen, T.-S. Chan, Y. Tan, *Adv. Energy Mater.* **2020**, Ahead of Print. DOI: 10.1002/aenm.202001364

[25] W. Kong, F. Gong, Q. Zhou, G. Yu, L. Ji, X. Sun, A. M. Asiri, T. Wang, Y. Luo, Y. Xu, J. *Mater. Chem. A: Materials for Energy and Sustainability* **2019**, *7*, 18823

[26] C. Wang, X,-D. Zhu, P.-J. Zuo, *Chem. Eng. J.* **2020**, *396*, 125163.

[27] D. Bao, Q. Zhang, F. Meng, H. Zhong, M. Shi, Y. Zhang, J. Yan, Q. Jiang, X. Zhang, *Adv. Mater.* **2017**, *29*, 1604799

[28] J. Wang, X. Feng, L. Yu, H. Xin, L. Hu, G. Chen, *Nature Comm.* **2018**, *9*, 1795.

[29] H.-M. Liu, S.-H. Han, Y. Zhao, Y.-Y. Zhu, X.-L. Tian, J.-H. Zeng, J.-H. Jiang, B. Y. Xia, Y. Chen, *J. Materials Chemistry A: Materials for Energy and Sustainability* **2018**, *6*, 3211

[30] S. Li, D. Bao, M. Shi, B. Wulan, J. Yan, Q. Jiang, *Adv. Mater.* **2017**, *29*, 1700001.

[31] X. Zhang, Q. Liu, X. Shi, A. M. Asiri, Y. Luo, X. Sun, T. Li, *J. Materials Chemistry A: Materials for Energy and Sustainability* **2018**, 6, 17303

[32] C. Lv, C. Yan, G. Chen, Y. Ding, J. Sun, Y. Zhou, G. Yu, *Angew. Chem., Int. Ed*. **2018**, *57*, 6073

[33] J. Han, Z. Liu, Y. Ma, G. Cui, F. Xie, F. Wang, Y. Wu, S. Gao, Y. Xu, X. Sun, *Nano Energy*, **2018**, *53*, 264

[34] J. Han, X. Ji, X. Ren, G. Cui, L. Li, F. Xie, H. Wang, B. Li, X. Sun, *J. Mater. Chem. A,* **2018**, *6*, 12974

[35] L. Zhang, X.-Y. Xie, H. Wang, L. Ji, Y. Zhang, H. Chen, T. Li, Y. Luo, G. Cui, X. Sun, *Chem. Commun*. **2019**, *55*, 4627

[36] X. Wu, L. Xia, Y. Wang, W. Lu, Q. Liu, X. Shi, X. Sun, *Small* **2018**, *14*, 1803111

[37] L. Cong, Z. Yu, F. Liu, W. Huang, *Catal. Sci. Technol*. **2019**, *9*, 1208

[38] K. Chu, Y-p. Liu, Y-b. Li, Y-l. Guo, Y. Tian, H. Zhang, *Appl. Catal. B* **2020**, *264*, 118525.

[39] K. Chu, Y-p. Liu, Y-b. Li, Y-l. Guo, Y. Tian, *ACS Appl. Mater. Inter.* **2020**, *12*, 7081-7090.

[40] K. Chu, J. Wang, Y-p. Liu, Q-q. Li, Y-l Guo. *J. Mater. Chem. A* **2020**, *8*, 7117-7124.

[41] K. Chu, Q.-q. Li, Q-qi. Li, Y-h. Cheng, Y-p. Liu, *ACS Appl. Mater. Interfaces* 2020, *12*, 11789–11796